Complexing Additives to Reduce the Immiscible Phase Formed in the Hybrid $ZnBr_2$ Flow Battery

D. Bryans, *,z **B. G. McMillan, M. Spicer, A. Wark, and L. Berlouis****

WestCHEM, Department of Pure & Applied Chemistry, University of Strathclyde, Glasgow G1 1XL, United Kingdom

The zinc-bromine redox flow battery (RFB) is one of a very few commercially viable RFB energy storage systems capable of integration with intermittent renewable energy sources to deliver improved energy management. However, due to the volatility of the electrogenerated bromine and potential for its crossover from positive to negative electrolytes, this system requires the use of quaternary ammonium complexes (*N*-methyl-*N*-ethylpyrrolidinium, (MEP)) to capture this bromine. This produces an immiscible phase with the Br_2 which requires a complex network of pipes, pumps and automated controls to ensure access to the electroactive material during discharge. In this work, the use of novel quaternary ammonium complexes to capture the electrogenerated bromine but to keep it in the aqueous phase is examined. Three compounds, 1-(carboxymethyl) pyridine-1-ium, 1-(2-carboxymethyl)-1-methylmorpholin-1-ium and 1-(2-carboxymethyl)-1-methylpyrrolidin-1-ium, were found to successfully reduce the volume of the immiscible phase formed on complexing with the polybromide (Br_x^-) whilst displaying similar enthalpy of vaporization values as that of MEP. Electrochemical analysis also revealed that these compounds did not impact on the electrode kinetics of the Br^-/Br_x^- reaction indicating that the resulting surface film formed with these compounds behaved as a chemically modified electrode, in contrast to the surface film formed with MEP.

Manuscript submitted August 14, 2017; revised manuscript received October 12, 2017. Published November 2, 2017. This was Paper 220 presented at the New Orleans, Louisiana, Meeting of the Society, May 28–June 1, 2017.

Renewable energy features in many countries' energy agendas. Current political focus seeks to reduce carbon emissions, as agreed by the Paris Agreement, by using energy more efficiently and to have power generation from zero carbon technologies.[1] Installed capacity of renewable energy sources have increased over the decade to 2014 by 175 GW for solar and by 322 GW for wind.[2] This increase in capacity has impacted on the global share of energy from renewable sources (excluding hydropower) from 2.2% (2004) to 9.7% (2013) with many countries promising to accelerate their installation of these technologies in the coming years.[3]

However, energy supplied from renewable sources is often intermittent and can fluctuate depending on weather and location.[4,5] This creates a problem in that energy can be generated in excess or in deficit in relation to energy demand. To solve this issue, energy storage is required to balance these peaks and troughs in order to stabilize energy flow into the electrical grid. This would lead to a better management of renewable sources.[6]

Redox flow batteries (RFBs) are one means of achieving large scale energy storage which can provide a more efficient link between energy production and energy demand. This type of battery system has the advantage of having a lower cost, a low level of self-discharge and is considered to have a much safer operation compared to other battery systems such as the sodium sulfur and lithium ion batteries.[7,8] Additionally, as with all batteries, it has the advantage of being more flexible and mobile in relation to pumped hydro and compressed air technologies since these large scale energy management technologies are restrained by the suitability of the terrain whereas RFBs are readily installed anywhere.[9,10]

The RFB typically consists of two external reservoirs, one for each half-cell, which store the positive and negative electrolytes of the battery. The total volume and concentration of the electrolyte has a direct impact on a particular system's energy storage capacity.[5,11] The power of the battery, on the other hand, is determined by the number of membrane electrode assemblies (cell pairs) in the stack. This decoupling of energy capacity and power output is highly desirable as this allows for tailored design of RFBs to satisfy a particular requirement.

Due to the above, the number of research publications on RFBs as well as their commercial development and deployment have increased over the last decade.[11–14] A particular good example of this is the zinc-bromine flow battery. This is described as a hybrid RFB as the formation of a new phase, Zn, takes place at the negative electrode during charging and so, the capacity of the battery is determined by the amount of zinc deposited rather than the volume of the negative electrolyte (Figure 1). Nevertheless, this is one of the cheapest RFBs available due to the low cost of its active material, zinc bromide. The use of zinc as the negative electrode redox couple also means that it also has a larger cell potential than most other aqueous-based systems, the half-cell reactions:[11]

$$Zn^{2+} + 2e^- \rightleftarrows Zn \quad E^0 = -0.76\ V\ vs.\ SHE$$

$$Br_2 + 2e^- \rightleftarrows 2Br^- \quad E^0 = +1.09\ V\ vs.\ SHE$$

giving a standard cell potential of 1.85 V (*c.f.* 1.26 V for the all-vanadium RFB). Extensive research has been conducted on this system in order to improve the overall performance or reduce the cost

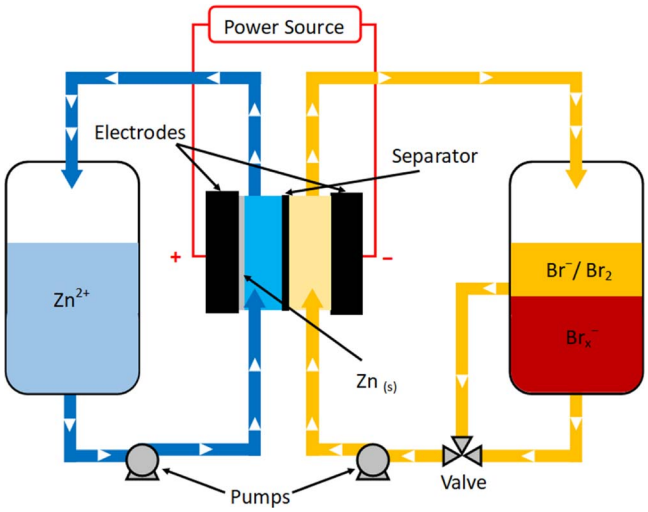

Figure 1. Simplified schematic of the zinc-bromine redox flow battery.

*Electrochemical Society Student Member.
**Electrochemical Society Member.
[z]E-mail: declan.bryans@strath.ac.uk

of this energy storage system. Innovations have included creating a cell pair without the requirement of a membrane and various electrode morphologies for enhanced activity.[15–17] However, most of the research has been focused on the two main issues associated with this RFB. The first is that of zinc dendrite formation, with studies ranging from simulations being conducted to improve the understanding of the zinc deposition to altering the fluid transport mechanics and the usage of additives to mitigate this problem.[18–20] The second major issue is associated with the electrogenerated bromine at the positive electrode which, at the upper limits of the operating temperature range of the cell (55°C) would have a substantial vapor pressure (B.Pt of liquid bromine is 58.8°C). The toxicity of bromine is well documented and the accumulation of its vapor in the positive reservoir headspace is highly undesirable since the element is very toxic by inhalation (LC_{50} 750 ppm 1 h (mouse)).[21] Furthermore, this loss of bromine to the vapor phase corresponds to loss in coulombic efficiency and so, to a reduction in the energy efficiency of the system. In order to prevent this from occurring, additives (Q^+ Br_x^-) are used to complex with the electrogenerated bromine. These additives are typically quaternary ammonium compounds that capture the Br_2 and complex this to high polybromide forms (e.g. Br_3^-, Br_5^- or Br_7^-).[22] Normally, the Q^+ Br_x^- yields an immiscible liquid phase which requires these battery systems to have additional pumping procedures to the positive electrode during discharge. The complexation of the Br_2 also serves to reduce the ability of the Br_2 to cross through the separator and react with the electroplated zinc metal at the negative electrode (another coulombic efficiency loss), a common problem that affects other bromine-based energy storage systems e.g. vanadium-bromine, hydrogen-bromine and polysulfide-bromine.[23–25] Currently, *N*-methyl-*N*-ethylpyrrolidinium bromide (MEP) is the complexing agent of choice used in commercial zinc bromine batteries.[26–28]

There is still nevertheless considerable interest in developing novel Q^+ Br_x^- compounds that could lead to improvements in the cycling efficiencies, kinetics, cost of materials or physical nature of complexed polybromide phase achieved.[29–31] Very few papers focus on the immiscible phase itself other than giving an analysis of the electrokinetics.[32,33] However, the mass transport issues created by having the secondary phase have been recognized by Yang et al.[34] In that study, surfactants were employed to break up the immiscible phase in order to improve its dispersion within the aqueous electrolyte. Using a small quantity of a polysorbate (polysorbate 20), they managed to increase the dispersion of the polybromide complex phase within the aqueous phase, leading to an increase in the coulombic efficiency.

The focus of the present work is to develop and characterize novel Q^+ Br_x^- that will form a complex with the electrogenerated bromine but remain in the aqueous phase, i.e. with minimal formation of an immiscible phase. This would improve the Br_x^- containing material's ability to disperse throughout the solution and reduce the complexity of the pumping requirements in these batteries. As with the MEP, it should also address the issue of free bromine crossover to the negative electrode compartment. One study carried out examined new complexes generated by the addition of hydroxyl functional groups to the current set of organic compounds (e.g. pyrrolidinium and morpholinium) employed in order to investigate their impact on charge-discharge cycling efficiencies as well as on the zinc deposition reaction.[29] In the present work, novel Q^+ Br_x^- have been synthesized and characterized for their impact on the Br_2/Br^- electrochemical kinetics as well as on their ability to capture and retain the electrogenerated bromine within the aqueous phase of the positive electrolyte.

Experimental

Materials.—The following compounds, 3-chloropropanoic acid, ethyl acetate, 1-methylpyrrolidine and 2-propanol used in the additive synthesis were obtained from Sigma-Aldrich. The 2-bromoacetic acid and pyridine were obtained from Alfa Aesar, while 4-methylmorpholine was obtained from Fluka.

The $ZnBr_2$ electrolyte, consisting of zinc bromide anhydrous (≥98%), potassium chloride (≥99%) and 1-methyl-1-ethylpyrrolidinium bromide (99%) were obtained from Sigma-Aldrich.

Bromine liquid was obtained from Acros Organics. Potassium iodide (99.8%) used for the iodometric titrations was supplied from Fisher Scientific and the sodium thiosulfate (99%) was obtained from Laboratory FSA Supplies. The latter was used for both the iodometric titrations and as a neutralising agent for any waste/spilled bromine during the experiments.

Synthesis.—The set of novel complex additives were synthesized based on two rationales:

1 – they were to have the same cyclic structure as other successful complex additives already identified (pyridine, morpholine and pyrrolidine).;[35,26,29] and 2, –the longer aliphatic leg of the quaternary ammonium compound was to incorporate a carboxylic acid functional group: known for improving the compound's solubility.[36,37]

These criteria led to the synthesis of compounds QBr1, QBr2 and QBr3. Figure 2 displays the structures of the synthesized quaternary ammonium additives employed in this study. Compound QBr1 was synthesized by refluxing 1 molar equivalent of pyridine with 1 molar

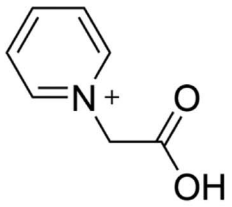

1-(carboxymethyl) pyridine-1-ium
(QBr1)

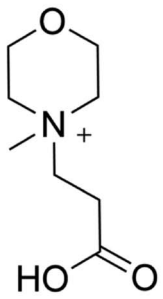

1-(2-carboxymethyl)-1-methylmorpholin-1-ium
(QBr2)

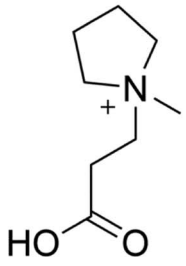

1-(2-carboxymethyl)-1-methylpyrrolidin-1-ium
(QBr3)

Figure 2. Chemical structures and names of novel additives.

equivalent of 2-bromoacetic acid in 40 mL of ethyl acetate for 4 h. The remaining solvent was removed in a desiccator leaving the precipitated product. Compounds QBr2 and QBr3 were synthesized by reacting 1 molar equivalent of 4-methylmorpholine and 1-methylpyrrolidine, respectively, with 1 molar equivalent of 3-chloropropanoic acid for 4 h. The precipitated compounds were purified by washing the salts with diethyl ether, vacuum filtered and dried in a vacuum oven at low temperature (60°C).

All of the synthesized quaternary ammonium additives were characterized using ^{1}H and ^{13}C NMR and mass spectroscopy. The ^{1}H and ^{13}C NMR (600 MHz) were recorded in deuterated DMSO.

Electrochemical analysis.—The electrochemical characterization was carried out in a small (~35 mL) 3-electrode glass cell. In this cell, the Pt mesh counter electrode (CE) was separated from the working electrode (WE) compartment by a porous glass frit (Grade 1). Electrolyte contact with the saturated (KCl) calomel reference electrode (SCE) was via a Luggin capillary which was positioned close to the WE's surface. The electrodes were connected to a computer-controlled Solartron S1 1287 Electrochemical Interface. The initial cyclic voltammograms were ran at a scan rate of 20 mV s^{-1} between the potential limits of 0.1 V and 1.3 V. A glassy carbon WE was used in a solution containing 50 mM $ZnBr_2$, 16.67 mM Q^+ Br_x^-, 0.5 M KNO_3. The cyclic voltammograms were used to examine the Br^- oxidation and subsequent Br_2 reduction and also determine the potential regions to use in the subsequent electrochemical impedance spectroscopy (EIS) and potentiodynamic measurements. Using the Solartron 1255B Frequency Response Analyser with 1287 electrochemical interface, the EIS was recorded in each electrolyte solution at pre-determined potentials over the frequency range of 1,000 Hz to 0.1 Hz. The potentiodynamic measurements (Tafel extrapolation) were carried out between 0.5 V–1.3 V at a scan rate of 0.1667 mV s^{-1}. Unless stated otherwise, the electrochemical measurements were carried out at 22°C ± 1°C.

Physical properties.—The complexing ability of the Q^+ Br_x^- additive with Br_2 was investigated by examining its ability to capture and hold the bromine into the aqueous phase. The samples used to conduct these tests were prepared by equilibrating these with a concentrated bromine solution (0.131 M) in the 3:1 molar ratio of Br_2: Q^+ Br_x^-. Subsequently, the vapor formed above the aqueous solution and the immiscible layer were analyzed for their bromine content in order to construct the Clausius-Clapeyron plots.[38]

The different components were added to a sealed sample bottle, filling a third of the bottle volume. The bottle was placed in a water bath where the temperature was controlled to ±0.5°C over the range of 20°C to 40°C. The Br_2 concentration in the vapor above the liquid component was measured using the Shimadzu UV-1800 UV Spectrophotometer, taking into account the absorptivity of the bromine. Once the set temperature was reached the sample bottle was equilibrated for 10 minutes prior to UV-Vis measurements. The temperature dependence of the Br_2 vapor pressure above both the aqueous and immiscible phases was measured in this manner and this allowed the enthalpy of vaporization (ΔH_{vap}) to be determined through the Clausius-Clapeyron equation. The data from these measurements was confirmed by repeating the experiment using an isoteniscope.[39] However, the method involving the UV-Vis spectrometer was preferred here as the isoteniscope measures the vapor pressure of both the Br_2 and the water whereas the UV-Vis spectrum only examines the Br_2 content.

For quantification of the Br_2 content in the aqueous phase, a 0.5 cm^3 aliquot of the solution from this layer was extracted. This aliquot was then added to a round-bottomed flask with 25 cm^3 of 0.5 M potassium iodide (excess). Sodium thiosulfate was employed as the titrant to the iodine generated by the reaction between the iodide and the bromine. The sodium thiosulfate (0.01 M) titrant was added at a known flow rate into this solution from a burette. Two small platinum electrodes, at a fixed distance apart, were placed into the solution and a very small current (50 nA) was passed between them. The potential difference between these two electrodes provided the end-point indicator, since as long as both the iodine and iodide were present at the electrodes, the potential remained steady. However, this potential difference rapidly rose when all the iodine was consumed by the reaction with the sodium thiosulfate.

Finally, the immiscible phase containing the Br_2 captured by the Q^+ Br_x^- additive was analyzed through Raman spectroscopy (Renishaw RM1000 microscope system with 633 nm HeNe excitation). This was done by extracting a small sample of the immiscible liquid and using a Ventacon macrosampler attached to the objective turret to focus light into a 1 mm glass cuvette via a Nikon MPlan 20 × NA 0.4 LWD objective. An integration time of 10 s was used. The presence of both Br_3^- and Br_5^- species could be identified from the Raman spectra.[33] By normalizing the data to the Br_3^- peak, the effectiveness of each of the Q^+ Br_x^- synthesized to capture the Br_2, based on the Br_5^- content, could be compared.

Results and Discussion

The initial tests investigated the impact that MEP had on the electrokinetics of the Br^-/Br_2 reaction in the 50 mM $ZnBr_2$ in 0.5 M KNO_3 electrolyte solution. Cyclic voltammetry was used to determine the effects that these complexes had on the reversibility of the reaction and also to identify the potential range to be used for subsequent electrochemical analysis.[40] Figure 3 shows the cyclic voltammetry in the absence and presence of a 16.67 mM concentration of the additives MEP, QBr1, QBr2 or QBr3. At the GC electrode, the Br^- oxidation reaction led to a diffusion-controlled current peak at ca. 1.22 V and the reverse Br_2 reduction gave a peak at ca. 0.62 V. Such a large peak separation indicates that the Br^-/Br_2 reaction at the GC electrode is electrochemically irreversible. Improved electron transfer kinetics for this couple can be obtained by carrying out the reaction using halogenated graphene electrodes where the anodic-cathodic peak separation is reduced to 150 mV or GC electrodes modified with single wall carbon nanotubes (60% purity) when the peak separation obtained is as low as 90 mV.[41,42] The anodic/cathodic peak current ratio (I_a/I_c) obtained from the data in Figure 3 is superior to unity (ca. 1.25–1.28) for all the voltammograms, again reflecting the irreversibility of the reaction at the GC electrode. The Br_2 reduction peak in the presence of MEP is higher than for all the other systems but also occurs at a more negative potential. The increase in the required overpotential could simply arise as a consequence of a surface film attenuating the applied potential. The shape of the reduction peak also suggests the presence of a surface controlled reaction with a rapid loss of active species beyond the current peak. This behavior is similar to that seen in metal stripping peaks where the reaction is a surface controlled process.[43–45]

Although the additives QBr1, QBr2 and QBr3 all produced very similar cyclic voltammograms in terms of the size and position of both the oxidation and reduction peaks, visual inspection of the glassy carbon electrode after the voltammograms with these additives indicated that a surface coating was also present, despite their reductive peaks maintaining a diffusion controlled profile. This would indicate then that the Br_2-containing complexes formed with the QBr1, QBr2 and QBr3 additives are indeed mostly found in the aqueous solution and diffuse to the electrode surface to be reduced. The film observed on the surface of the electrode then acts as a chemically modified electrode and does not influence the electrode kinetics of the Br^-/Br_2 reaction. This would indicate then that the complexes are indeed performing their designed function of capturing the electrogenerated bromine and retaining them in the aqueous phase. The electrode kinetics of each system were further investigated using EIS and potentiodynamic measurements.

Figure 4 shows the EIS spectra carried out in the solutions with and without MEP at the half-wave potential, $E_{\frac{1}{2}}$. Clearly, in the presence of MEP, the size of the 'semi-circle' was significantly smaller. The data in Table I were obtained by fitting an equivalent circuit comprising of a resistance (R_s) in series with a parallel R_{CT} $-W$ $/C_{CPE}$ circuit, corresponding to the uncompensated solution resistance R_s between

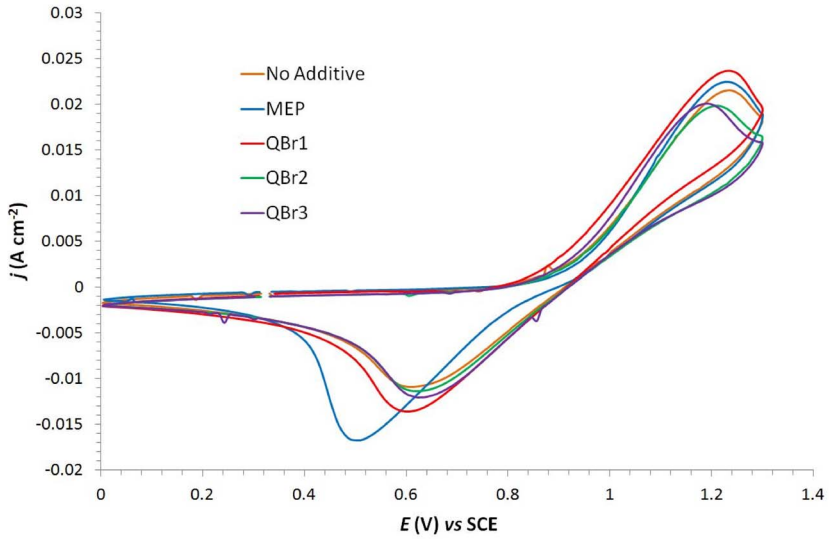

Figure 3. Cyclic voltammograms at a glassy carbon electrode in 50 mM $ZnBr_2$, 0.5 M KNO_3 with 16.67 mM of either MEP, QBr1, QBr2 or QBr3. Scan rate of 50 mV s^{-1}. $T = 295$ K.

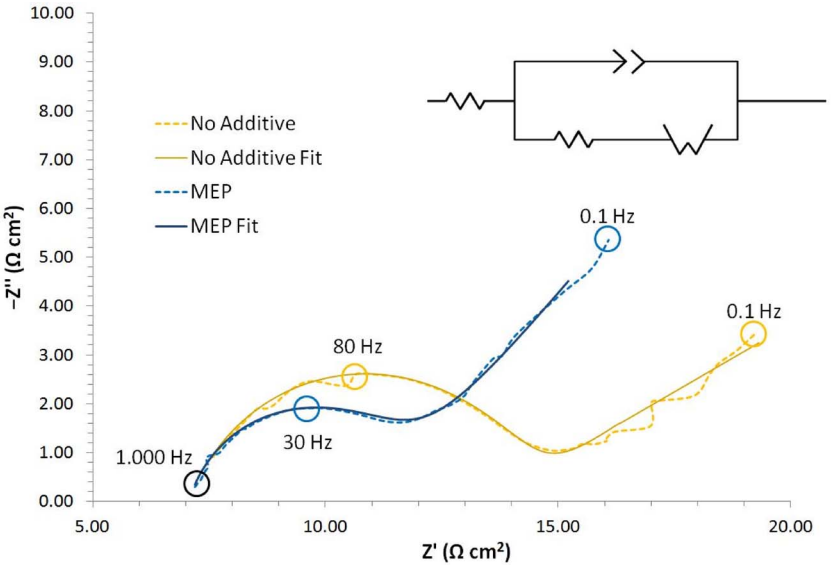

Figure 4. EIS data obtained at $E_{\frac{1}{2}}$ in the solution containing 50 mM $ZnBr_2$, 0.5 M KNO_3 with no additive (orange) and with 16.67 mM MEP (blue) at a GC electrode. $T = 295$ K. Inset shows equivalent circuit used for fitting the data.

the RE and WE, the charge transfer resistance R_{CT}, a constant phase element *CPE* and a Warburg diffusional impedance, *W*. This data reveals that the double layer capacitance (obtained from *CPE* and R_{CT}) is almost 5 times larger for MEP than that observed in the solutions with no additives or with the solutions containing QBr1, QBr2 and QBr3. This indicates that the MEP layer that is formed on the electrode surface once charged with the Br_2 is a complete homogeneous one holding the Br_x^- electroactive species at the electrode surface but that the ones formed with the QBr1, QBr2 and QBr3 additives is more loosely bound so that the reduction of the Br_x^- species is controlled by diffusion back to the electrode surface.

The trend in the R_{CT} values in Table I is consistent with the above discussions. The ready availability of the Br_x^- species in the case of MEP at the surface would mean that the electron transfer step could occur more readily (lower R_{CT}). In the case of the QBr1, QBr2 and QBr3 additives, since the complexes formed are much more soluble, the surface concentration of available Br_x^- is lower which impacts then on the R_{CT} values. Indeed, for QBr2 and QBr3 complexes, the R_{CT} values are larger than for the aqueous solution with no additive, suggesting that there is actually a slight inhibition of the electron transfer step with these compounds. The values for the Warburg coefficient obtained from the fitted data indicate a lower effective diffusion

Table I. Electrochemical data from analysis of electrolyte solutions (50 mM $ZnBr_2$, 0.5 M KNO_3, 16.67 mM of $Q^+Br_x^-$) with no additive, MEP and Compounds QBr1, QBr2 and QBr3. Warburg coefficient is represented in the table as σ.

	Tafel Extrapolation			EIS		
Compound	B_a (mV)	j_0 (mA cm^{-2})	E_0 (mV)	R_{CT} (mA cm^{-2})	C_{dl} (μF cm^{-2})	σ (Ω cm^2 $s^{-1/2}$)
No QBr	62.3	0.108	0.84	7.6	295	1.85
MEP	71.6	0.304	0.115	5.4	1069	4.26
QBr1	54.3	0.115	0.84	6.3	401	1.42
QBr2	50.1	0.092	0.84	8.3	296	3.21
QBr3	50.2	0.101	0.84	8.5	321	2.96

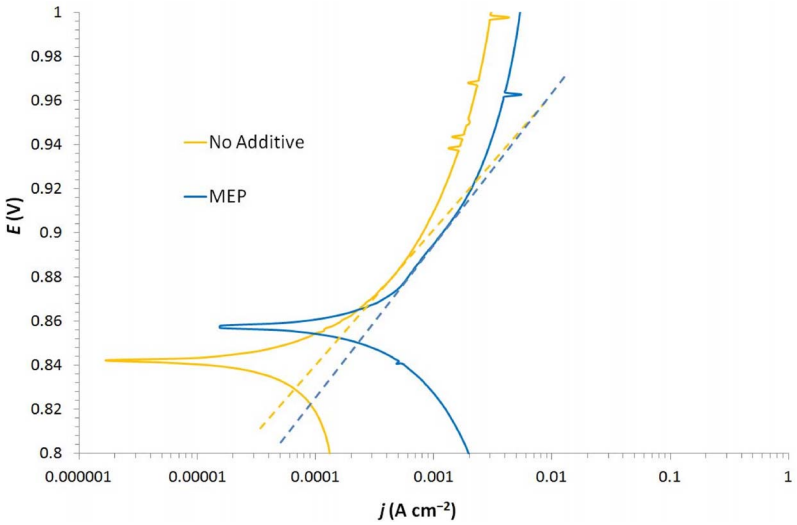

Figure 5. Tafel slopes (dashed lines) obtained from potentiodynamic curves in a solution containing 50 mM $ZnBr_2$, 0.5 M KNO3 with no additive (orange) and with 16.67 mM MEP (blue).

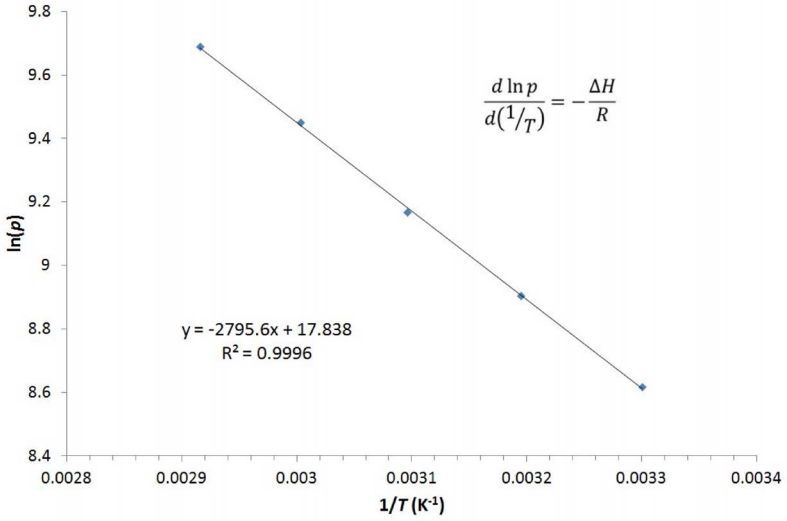

Figure 6. Plot of ln p_{Br2} against $1/T$ for QBr2.

coefficient ($\sigma \propto 1/D^{\frac{1}{2}}$) for the solution containing MEP compared to the other additives, in line with the above discussion. The results from the potentiodynamic measurements (Tafel extrapolation) shown in Table I indicates that MEP has over twice the exchange current density, j_o value, compared to the other additives or the solution with no additive, as also evidenced from the EIS data above. The anodic Tafel slope B_a for the bromide oxidation reaction with no additives is close to the ideal value (~60 mV) for a 2-electron transfer with an anodic charge transfer coefficient α_A of 0.5, as seen in Figure 5. With the MEP present, B_a increases slightly to 72 mV but decreases to <55 mV in the presence of the QBr1, QBr2 and QBr3 compounds. This would suggest small changes in the value of α_A, reflecting the impact that complexation has on the product of the oxidation reaction.

The relatively low concentrations required for the refined electrochemical characterization did not however permit the full physical interactions between the Q^+ Br_x^- compounds and the bromine to be determined. In order to examine this, a molar ratio of 3:1 bromine to additive was used when carrying out these studies, with the aqueous bromine concentration being 0.131 M. In these tests, immediate differences could be seen between the various Q^+ Br_x^- mixtures, with the solution containing MEP producing a dense, deep red immiscible phase which had the viscosity of that comparable to oil and no significant bromine vapor above aqueous phase. The aqueous solution containing no additives on the other hand had the intense orange color associated with the Br_2 and this was also clearly evident in the vapor above the solution. With the QBr1, QBr2 and QBr3 mixtures however, it was observed that the volume of immiscible liquid formed was indeed significantly reduced, in accordance with the original expectations of the work. Again here, the Br_2 vapor presence above the aqueous phase was insignificant. To verify that the bromine was coupled into a soluble complex within these aqueous phases (as well as in the small volume of the immiscible phase), these phases were analyzed for their bromine content and the enthalpy of vaporization was measured so that they could be directly compared to MEP. Table II summarizes the enthalpies of vaporization found and the Br_2 content of the aqueous phase for each of the Q^+ Br_x^- compounds after equilibration with aqueous bromine solution. The enthalpy of vaporization

Table II. Data showing enthalpy of vaporization for Br_2 from the immiscible phases formed with MEP and Q^+ Br_x^- compounds and the concentration of Br_2 remaining in the aqueous phase.

Compound	ΔH of Vaporization		Free Br_2
	Oil Phase (kJ mol^{-1})	Aqueous Phase (kJ mol^{-1})	concentration (mol dm^{-3})
No QBr	N/A	15.9	0.131
MEP	37.8	21.6	0.061
QBr1	27.8	19.1	0.065
QBr2	33.2	23.2	0.065
QBr3	N/A	29.7	0.062

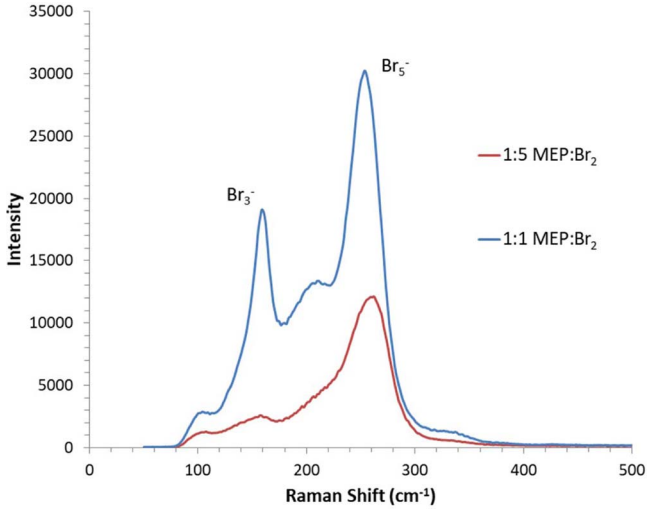

Figure 7. Raman spectra of a concentrated bromine solution with either 1:1 (blue) or a 1:5 (red) molar equiv. of MEP. $T = 295$ K.

of Br_2 was determined from the Clausius-Clapeyron equation as discussed in the Experimental section. The data of Figure 6 shows that an excellent fit was obtained to the data, in this case for the QBr2 additive but similar linear plots were obtained for all the systems examined. The enthalpy for the aqueous solution without MEP was found to be $\Delta H = 15.9$ kJ mol^{-1}. However, that for the aqueous solution with MEP was $\Delta H = 21.6$ kJ mol^{-1} indicating that that more energy was required to produce the Br_2 vapor from the aqueous phases which also contained MEP. The enthalpy of vaporization for Br_2 from the immiscible phase was expectedly larger at 37.8 kJ mol^{-1}. For the QBr1, QBr2 and QBr3 compounds, the enthalpy of bromine vaporization from the solution mixture containing QBr1 was slightly lower than that of MEP but for QBr2 and QBr3, the values were higher and significantly so for the latter, at 29.7 kJ mol^{-1} indicating that the complex in the aqueous phase is much more effective than MEP for holding the Br_2. Thus, as the data from the iodometric titrations also indicated that the free Br_2 concentration in the aqueous phase were very similar (0.063 ± 0.002 mol dm^{-3}) for all the additives, the increased enthalpy of vaporization measured for QBr2 and QBr3, with respect to that for MEP, is very encouraging.

The immiscible phases from all the solution mixtures were analyzed using Raman spectroscopy in order to determine the nature of the polybromide species present in that phase. Figure 7 shows the Raman spectra acquired from samples with the concentration ratio of 1:1 and 5:1 of Br_2: MEP. Two peaks can clearly be identified at ca. 160 cm^{-1} and ca. 250 cm^{-1} which correspond to the polybromide species Br_3^- and Br_5^-, respectively.[33] As expected, as the bromine content increases, the preferred polybromide species changes from Br_3^- to Br_5^-. In order to compare the effectiveness of the novel QBr1, QBr2 and QBr3 additives with MEP, the Br_3^- peak was normalized so as to allow the proportion of the higher polybromide state of Br_5^- to be

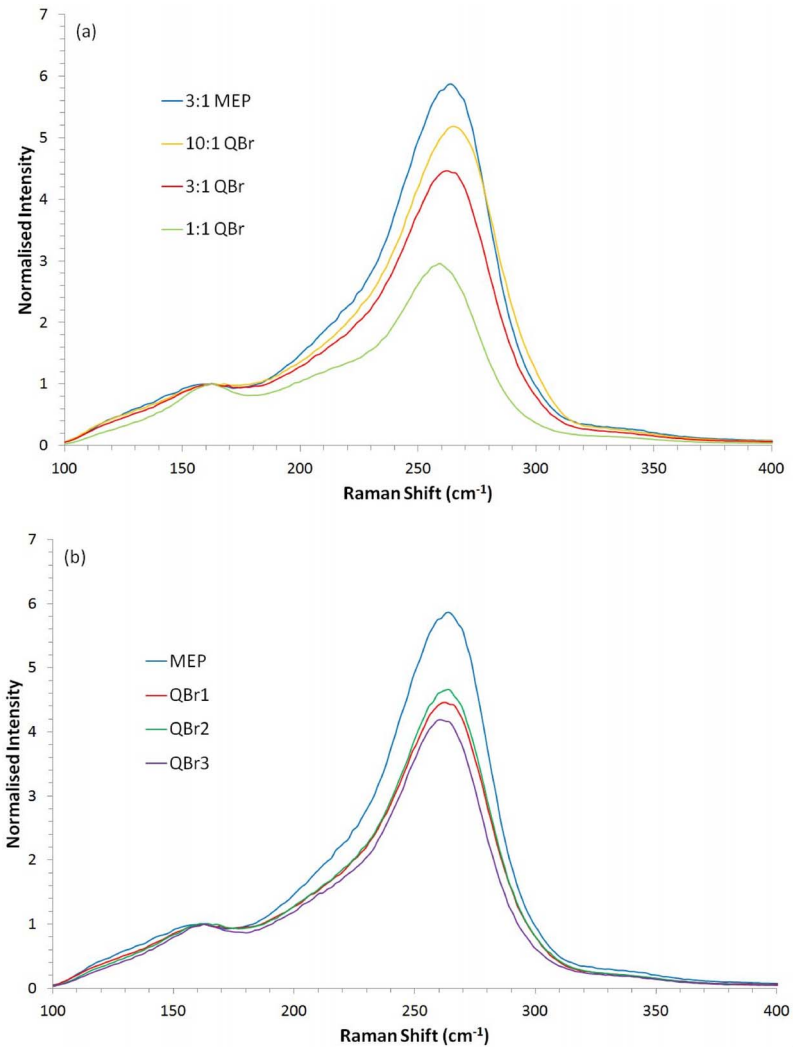

Figure 8. Raman spectra normalized to the Br_3^- signals, (a) comparing the Br_5^- signal from the immiscible phases formed with MEP, QBr1, QBr2 and QBr3 in the 3:1 Br_2: Q^+ Br_x^- ratio and (b) comparing the impact of different concentration ratios for QBr1 with that of 3:1 MEP. $T = 295$ K.

emphasized. Figure 8a shows that for the same concentration ratios MEP still proves to be superior in forming the Br_5^- state. In fact, Figure 8b shows that despite varying the concentration of the QBr1 complex additive from a 1:1 ratio to a 10:1 ratio, MEP still enabled the formation of the Br_5^- complex to a greater degree.

Conclusions

Novel complexing additives for use in the Zn-Br_2 hybrid RFB were successfully produced using simple synthetic routes. The additives containing the carboxyl functional groups showed similar electrochemical properties to the $ZnBr_2$ solution with no additive present, showing that there was no inhibition of the electrochemical kinetics here. These formed much lower quantities of the immiscible phase in comparison to that of MEP in the concentrated aqueous bromine solutions indicating that the Q^+ Br_x^- complex formed were indeed much more soluble than that with MEP. This would improve the Q^+ Br_x^- 's ability to disperse throughout the solution and reduce the complexity of the pumping requirements in zinc-bromine redox flow batteries. These additives also displayed similar enthalpy of vaporizations and of aqueous bromine concentrations to that of MEP. Nevertheless, in the immiscible phase, MEP was capable of producing more of the higher order polybromide Br_5^- species than the other additives.

Acknowledgments

One of the authors (DB) would like to extend his gratitude to the Energy Technology Partnership and Lotte Chemical for sponsoring this work alongside the University of Strathclyde.

ORCID

D. Bryans https://orcid.org/0000-0002-7932-0626

References

1. Adoption of the Paris Agreement., *http://unfccc.int/resource/docs/2015/cop21/eng/l09r01.pdf*, Last visited 02/09/2017.
2. Ren21, *First Decad. 2004–2014, 10 Years Renew. Energy Prog.* ,*(http//www.ren21.net/Portals/0/documents/activities/TopicalReports/REN21_10yr.pdf)*, Last visited 02/09/2017.
3. Ren21, *Renewables 2015-Global Status Rep*., Last visited 02/09/2017.
4. H. Lund, *Energy*, **32**, 912 (2007).
5. H. Zhao, Q. Wu, S. Hu, H. Xu, and C. N. Rasmussen, *Appl. Energy*, **137**, 545 (2014).
6. Z. Yang, J. Zhang, M. C. W. Kintner-Meyer, X. Lu, D. Choi, J. P. Lemmon, and J. Liu, *Chem. Rev.*, **111**, 3577 (2011).
7. H. Sezer, M. Aygun, J. H. Mason, E. Baran, and I. Celik, *ECS Trans.*, **69**, 91 (2015).
8. P. Peng and F. Jiang, *Int. J. Heat Mass Transf.*, **103**, 1008 (2016).
9. M. Skyllas-Kazacos, M. H. Chakrabarti, S. a. Hajimolana, F. S. Mjalli, and M. Saleem, *J. Electrochem. Soc.*, 2011, **158**, R55.
10. P. Lex, *Power Eng. J.*, **13**, 142 (1999).
11. P. Leung, X. Li, C. Ponce de León, L. Berlouis, C. T. J. Low, and F. C. Walsh, *RSC Adv.*, **2**, 10125 (2012).
12. T. Shigematsu, *SEI Tech. Rev.*, **73**, 5 (2011).
13. W. Wang, Q. Luo, B. Li, X. Wei, L. Li, and Z. Yang, *Adv. Funct. Mater.*, **23**, 970 (2013).
14. A. Z. Weber, M. M. Mench, J. P. Meyers, P. N. Ross, J. T. Gostick, and Q. Liu, *J. Appl. Electrochem.*, **41**, 1137 (2011).
15. S. Biswas, A. Senju, R. Mohr, T. Hodson, N. Karthikeyan, K. W. Knehr, A. G. Hsieh, X. Yang, B. E. Koel, and D. A. Steingart, *Energy Environ. Sci.*, **334**, 928 (2017).
16. C. Wang, Q. Lai, P. Xu, D. Zheng, X. Li, and H. Zhang, *Adv. Mater.*, **29**, 2 (2017).
17. W. I. Jang, J. W. Lee, Y. M. Baek, and O. O. Park, *Macromol. Res.*, **24**, 276 (2016).
18. G. P. Rajarathnam and A. M. Vassallo, *SpringerBriefs in Energy*, 45 (2016).
19. H. S. Yang, J. H. Park, H. W. Ra, C. S. Jin, and J. H. Yang, *J. Power Sources*, **325**, 446 (2016).
20. S. J. Banik and R. Akolkar, *J. Electrochem. Soc.*, **160**, D519 (2013).
21. R. M. J. Withers and F. P. Lees, *J. Hazard. Mater.*, **13**, 279 (1986).
22. J. Noack, N. Roznyatovskaya, T. Herr, and P. Fischer, *Angew. Chemie - Int. Ed.*, **54**, 9776 (2015).
23. S. Winardi, G. Poon, M. Ulaganathan, A. Parasuraman, Q. Yan, N. Wai, T. M. Lim, and M. Skyllas-Kazacos, *Chempluschem*, **80**, 376 (2015).
24. K. Oh, A. Z. Weber, and H. Ju, *Int. J. Hydrogen Energy*, **42**, 3753 (2017).
25. P. Zhao, H. Zhang, H. Zhou, and B. Yi, *Electrochim. Acta*, **51**, 1091 (2005).
26. G. Poon, A. Parasuraman, T. M. Lim, and M. Skyllas-Kazacos, *Electrochim. Acta*, **107**, 388 (2013).
27. K. J. Cathro, K. Cedzynska, and D. C. Constable, *J. Power Sources*, **16**, 53 (1985).
28. J.-D. Jeon, H. S. Yang, J. Shim, H. S. Kim, and J. H. Yang, *Electrochim. Acta*, **127**, 397 (2014).
29. M. Schneider, G. P. Rajarathnam, M. E. Easton, A. F. Masters, T. Maschmeyer, and A. M. Vassallo, *RSC Adv.*, **6**, 110548 (2016).
30. D. Bryans, L. Berlouis, M. Spicer, B. G. McMillan, and A. Wark, *ECS Trans.*, **77**, 33 (2017).
31. G. P. Rajarathnam, M. E. Easton, M. Schneider, A. F. Masters, T. Maschmeyer, and A. M. Vassallo, *RSC Adv.*, **6**, 27788 (2016).
32. W. Kautek, a Conradi, C. Fabjan, and G. Bauer, *Electrochim. Acta*, **47**, 815 (2001).
33. G. Bauer, J. Drobits, C. Fabjan, H. Mikosch, and P. Schuster, *J. Electroanal. Chem.*, **427**, 123 (1997).
34. J. H. Yang, H. S. Yang, H. W. Ra, J. Shim, and J.-D. Jeon, *J. Power Sources*, **275**, 294 (2015).
35. E. Lancry, B. Z. Magnes, I. Ben-David, and M. Freiberg, *ECS Trans.*, **53**, 107 (2013).
36. D. S. Vicentini, R. V. Salvatierra, A. J. G. Zarbin, L. G. Dutrac, and M. M. Sá, *J. Braz. Chem. Soc.*, **25**, 1939 (2014).
37. R. Zhang and J. A. Moore, *Macromol. Symp.*, **199**, 375 (2003).
38. S. A. Tittlemier and G. T. Tomy, *Environ. Toxicol. Chem.*, **20**, 146 (2001).
39. S. N. Bajpal, *J. Chem. Eng. Data*, **26**, 2 (1981).
40. R. S. Nicholson, *Anal. Chem.*, **37**, 1351 (1965).
41. Y. Munaiah, P. Ragupathy, and V. K. Pillai, *J. Electrochem. Soc.*, **163**, A2899 (2016).
42. Y. Munaiah, S. Dheenadayalan, P. Ragupathy, and V. K. Pillai, *ECS J. Solid State Sci. Technol.*, **2**, M3182 (2013).
43. G. Nikiforidis, L. Berlouis, D. Hall, and D. Hodgson, *Electrochim. Acta*, **113**, 412 (2013).
44. F. Chen, Q. Sun, W. Gao, J. Liu, C. Yan, and Q. Liu, *J. Power Sources*, **280**, 227 (2015).
45. P. K. Leung, C. Ponce-De-León, C. T. J. Low, and F. C. Walsh, *Electrochim. Acta*, **56**, 6536 (2011).